Optical implementation of micro-zoom arrays for parallel focusing in integral imaging

A. Tolosa,[1] R. Martínez-Cuenca,[3] A. Pons,[2] G. Saavedra,[2] M. Martínez-Corral,[2,*] and B. Javidi[4]

[1]*Department of Color and Ophthalmic Optics, AIDO, 46980 Paterna, Spain*
[2]*3DDI Laboratory, Department of Optics, University of Valencia, E-46100 Burjassot, Spain*
[3]*GROC-UJI. Department of Physics, Universitat Jaume I, 12080 Castelló, Spain*
[4]*Electrical and Computer Engineering Department, University of Connecticut, Storrs, Connecticut 06269-1157, USA*
[*]*Corresponding author: manuel.martinez@uv.es*

Received July 24, 2009; revised January 8, 2010; accepted January 12, 2010;
posted January 13, 2010 (Doc. ID 114773); published February 23, 2010

We report 3D integral imaging with an electronically tunable-focal-length lens for improved depth of field. The micro-zoom arrays are generated and implemented based on the concept of parallel apodization. To the best of our knowledge, this is the first report of parallel dynamic focusing in integral imaging based on the use of micro-zoom arrays. © 2010 Optical Society of America

OCIS codes: 110.6880, 100.2000, 100.6890.

1. INTRODUCTION

Integral imaging (InI) is a very promising technique for the acquisition and display of images of 3D scenes. Based on an old concept published by Lippmann more than one century ago [1], InI produces autostereoscopic 3D images that can be observed directly with no need of additional viewing devices such as special glasses. The multiview nature of InI allows 3D color images to be viewed by multiple audiences [2,3]. Recently, the interest in the development of InI systems and its applications has increased rapidly, thanks to the research effort of many groups. This intense growth has focused mainly on optical design concerns [4–10]. Of course, these proposals have been directed to improve the performance of the technique in terms of resolution [11,12] and viewing angle [13,14]. Other important aspects that have been recently addressed are the production of 3D–2D convertible displays [15] or the extraction of 3D information from scenes [16,17]. More information about these techniques and its applications can be found in [18–20].

One aspect of InI development that, to the best of our knowledge, has not been investigated is the implementation of a technique for rapid and flexible refocusing of the recording or the display setup. The simplest solution to this problem is to reset the distance between the sensor (or the display device) and the microlens array. This solution is not very efficient because such resetting implies a distortion in the 3D scale of reconstructed images. Another solution could be the use an array of varifocal microlenses, like the ones fabricated by Ferraro *et al.* [21]. However, these micolenses cannot be used easily in an integral imaging device, since they require an environment of very low temperature. Instead, we propose a simple fully optical technique for production of a micro-zoom array. Our proposal takes profits from the parallel apodizing capacity of telecentric relay systems (TRES) [10]. A TRES device was originally proposed for the reduction of shifting and overlapping of elemental images during the capture stage, by projection of micro-entrance-pupils in front of any of the microlenses in the array. This device can be used for projection of any amplitude transmittance modulation for the microlenses and therefore for parallel apodization of the lenses. In this paper, we propose to project the transmittance of a lens of variable optical power to produce the micro-zoom array.

2. REVISITING THE TRES SCHEME

Let us start by revisiting the TRES concept. As described in [10], TRES allows all-optical implementation of perpendicular barriers between elemental cells. Such barriers prevent the overlapping between elemental images during the pickup process and also prevent the typical flipping effect during display. The experimental implementation of TRES is usually done by combining a large-diameter converging lens and a macro camera lens. The task of the large lens is twofold. One is collecting the light rays proceeding from the microlenses. The other is to confer to the relay system the necessary telecentricity. The telecentricity is achieved after allowing the aperture stop of the macro to be conjugate with infinity. To simplify the drawing, in Fig. 1(a) we have schematized the TRES through the afocal coupling of a large converging lens, named here the field lens, and a smaller converging lens (the sensor lens). Since the aperture stop of the TRES is placed at the back focal plane of the field lens, the entrance pupil is placed at infinity. The coupling between the microlens array and the TRES projects, in parallel, the entrance pupil of the TRES onto the front focal plane of any microlens. These projected pupils are the elemental entrance pupils (also named micro-entrance-pupils). The elemental entrance pupils restrict the rays impinging

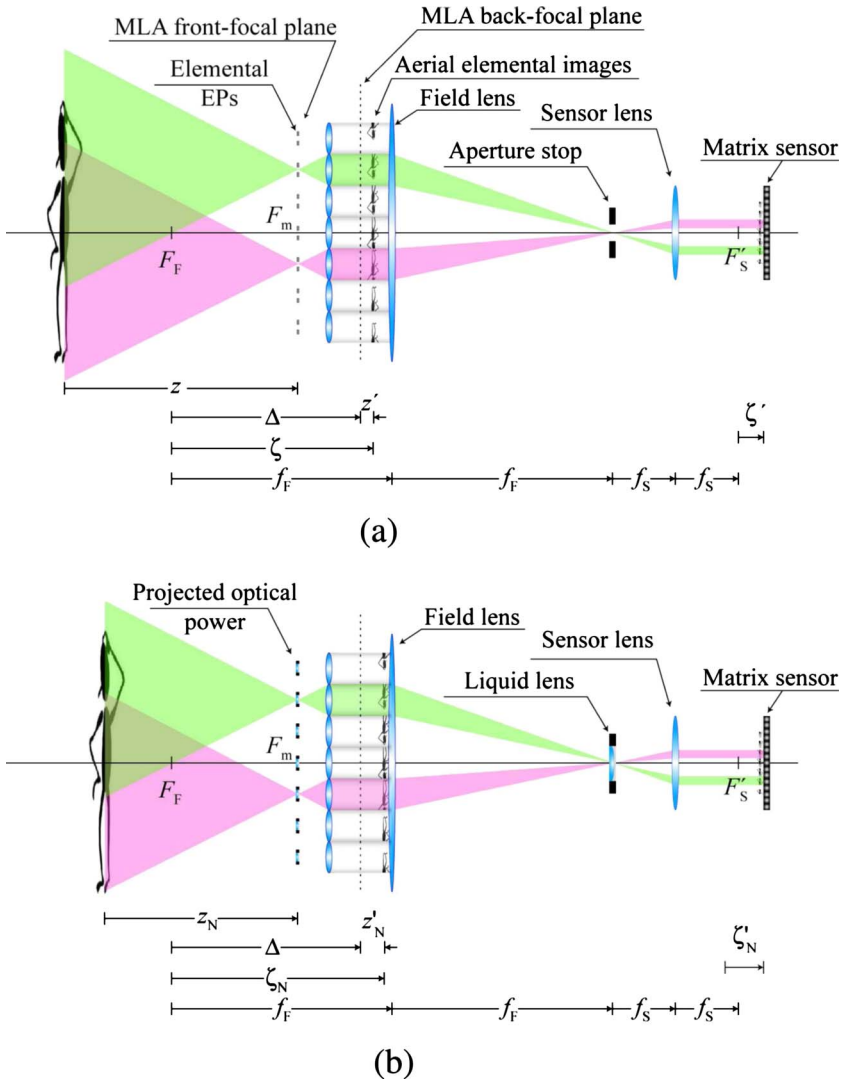

Fig. 1. (Color online) (a) Illustration of the TRES concept. Owing to the telecentricity of the relay system, the aperture stop is back-projected virtually onto the front focal plane of any microlens. Only rays passing through the projected micropupils and therefore emerging from the microlens parallel to its optical axis will reach the sensor. EPs, entrance pupils; MLA, microlens array. The matrix sensor is the camera. (b) When a lens is inserted at the TRES aperture stop, the lens optical power is projected in parallel in front of any microlens.

on each microlens so that only rays emerging from the microlens that are parallel to its axis are allowed. Thus, perpendicular barriers are implemented by a pure optical method.

Next, we deduce conjugation equations of this multiple imaging system, i.e., the equations that relate the position and size of the object to the position and size of recorded elemental images. Δ denotes the distance between the front focal plane of the field lens and the back focal planes of the microlenses. By use of Newton's equation for conjugate distances [22] one finds that for the case of an object placed at distance z from the front focal plane, F_m, of the array, a collection of aerial elemental images are produced at the distance

$$z' = f_m^2/z \tag{1}$$

from the back focal plane of the microlenses. Here f_m is the focal length of any microlens. The magnification of this imaging is

$$M_m = -f_m/z, \tag{2}$$

where the minus sign indicates that the aerial images are inverted.

The aerial elemental images are then imaged through the telecentric coupling onto the sensor plane. Using the conjugation equations for an afocal arrangement [22], which take the reference for the axial distances in a pair of conjugate planes, we find that [see Fig. 1(a)]

$$\zeta' = \zeta M_T^2 = (z' + \Delta)M_T^2, \tag{3}$$

where $M_T = -f_S/f_F$ is the lateral magnification of the TRES.

Expressed in different manner, if we fix ζ' as the distance from F'_S to the sensor, the in-focus plane of the overall system is then set at a distance z (to F_m) such that

$$\frac{1}{z} = \frac{1}{f_m^2}\left(\frac{\zeta'}{M_T^2} - \Delta\right). \tag{4}$$

Naturally, the overall magnification of this parallel imaging process is given by the product

$$M = M_m M_T = \frac{1}{z}\frac{f_m f_S}{f_F} = \left(\frac{\zeta'}{M_T^2} - \Delta\right)\frac{f_S}{f_m f_F}. \quad (5)$$

3. MICRO-ZOOM ARRAY

Let us suppose now that, instead of a clear circular aperture, we insert at the TRES aperture stop a lens whose refractive power can be controlled electronically, between certain limits [see Fig. 1(b)]. We name the focal length of such lens f_L (which will be called hereafter the liquid lens). Besides, we assume that the distance between the sensor lens and the sensor remains fixed. By application of geometrical optics [22], we find that the focal length of the coupling between the liquid lens and the sensor lens is still f_S. The front focal plane of the coupling appears at the liquid lens position, whereas the back focal plane is at a distance $f_S - f_S^2/f_L$ from the sensor lens. Then the new distance, ζ'_N, between the back focal plane of the coupling and the sensor is given by

$$\zeta'_N = \zeta' + f_S^2 \varphi_L, \quad (6)$$

where $\varphi_L = 1/f_L$. Now it is straightforward to find that the new in-focus plane for the integral imaging system is at a distance z_N such that

$$\frac{1}{z_N} = \frac{1}{z} + \left(\frac{f_F}{f_m}\right)^2 \varphi_L. \quad (7)$$

The overall magnification of the multiple-imaging system is changed, as well. The new value, M_N, can be calculated as

$$M_N = M + \frac{f_S f_F}{f_m}\varphi_L. \quad (8)$$

The same results could be obtained through Fourier optics reasoning by applying the parallel projection concept (see Appendix A).

4. EXPERIMENTAL VERIFICATION

To implement our technique we used the liquid lens Arctic 314 manufactured by Varioptic. This tunable liquid lens is based on electrowetting technology: the spreading of a drop of water on an electrically insulating surface can be modified by creating an accumulation of charges at the base of the drop. The densities of the two liquid phases are matched in order to keep the phases in place when the position of the lens changes. Then, the optical power of the resulting liquid lens can be tuned by application of proper electric voltage [23,24]. The nominal specifications for the Arctic 314 are shown in Table 1.

For our part, we have measured the optical power of the Arctic 314 as a function of the applied voltage. For the measurement we used the focimeter Axil manufactured by Essilor. As shown in Fig. 2, there is a linear relation between the optical power and the applied voltage in the range $\varphi_L \in [-5\ \mathrm{m}^{-1}, +12\ \mathrm{m}^{-1}]$. Note, however, that because of the high repeatability of the results, the Arctic 314 can be used even with an optical power outside the linear regime.

Table 1. Nominal Specifications of Liquid Lens Used for Experiments

Specification	Value
Minimum power	$-2\ \mathrm{m}^{-1}$
Maximum power	$+10\ \mathrm{m}^{-1}$
Wavefront distortion	80 nm
Transmission at $\lambda = 585$ nm	97%
Optical aperture	2.5 mm

For experimental verification, we inserted the liquid lens at the aperture stop of a camera lens combined with a large-diameter lens in telecentric manner [see Fig. 3(a)]. To make sure that the back focal plane of the large lens matches the entrance pupil of the camera lens, we placed an auxiliary digital camera, focusing to infinity, just in front of the large-diameter lens. Then, we adjusted the distance between the large lens and the camera lens so that a sharp image of the mount of the liquid lens was obtained at the sensor of the auxiliary camera [see Fig. 3(b)]. This image of the mount was used, as well, to determine, by simple pixel counting, the size of the imaged mount and, therefore, the focal length of the object side of the telecentric arrangement. The result of measurement was $f_F = 96.1$ mm ($\pm 1\%$).

Next we arranged the multiple-imaging setup by placing the microlens array just in front of the large lens [see Fig. 3(a)]. The lens array was composed of lenses of focal length $f_m = 10$ mm and diameter $\phi_m = 2$ mm, arranged in a hexagonal grid. We used a 3D scene consisting of two dice with different colors and sizes. Since the magnification of the system decreases with the distance to the lens array, we placed the smaller object closer to the lens array. Then, we adjusted the liquid power to $\varphi_L = 0$. With this setup, we obtained the elemental images shown in Fig. 4(a), in which both the red and the blue die were out of focus. By continuous variation of the optical power from $\varphi_L = 0$ to $\varphi_L = +10\ \mathrm{m}^{-1}$, we could tune at will the position of the in-focus plane, as shown in Fig. 4.

To clarify the focusing capabilities of the proposed system, we applied the back-projection technique described in [16] to reconstruct the scene at the in-focus plane. Specifically, we backprojected computationally each elemental image on the desired reconstruction plane through its unique associated pinhole. The collection of all the back-projected elemental images were then superimposed computationally to achieve the intensity distribution on the reconstruction plane. In particular, in Fig. 5 we show the images reconstructed from Fig. 4(a) and 4(b).

Although not confirmed experimentally by us we point out that the speed of the proposed system is determined by that of the Arctic 314 device. In particular, the characteristic response time of the lens is of the order of 10 ms, whereas the lens recovers its full quality after 50 ms [25]. As for the precision, we have not found such specific information in the literature, but we have confirmed (see Fig. 2) that the focal power of the varifocal lens can be fixed with a precision that far exceeds $0.25\ \mathrm{m}^{-1}$.

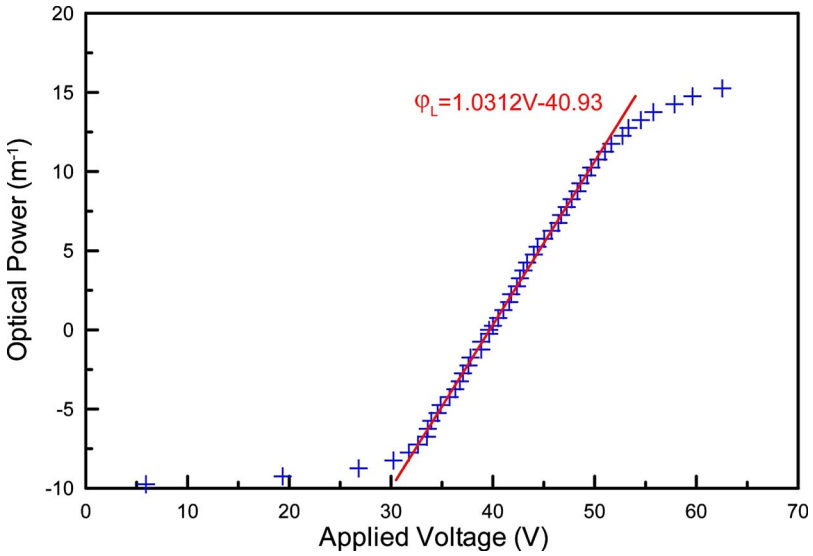

Fig. 2. (Color online) Measured relation between the optical power of the liquid lens and the applied voltage.

5. CONCLUSIONS

We have reported a 3D integral imaging system with electronically tunable-focal-length lens for improved depth of field. The approach is based on the telecentric relay systems [10] concept. We have presented a simple method for optical implementation of a particular case of parallel apodization. An array of micro-zoomlenses is synthesized optically by projecting onto the front focal plane of any microlens of the array the transmittance of a variable-focal-length lens.

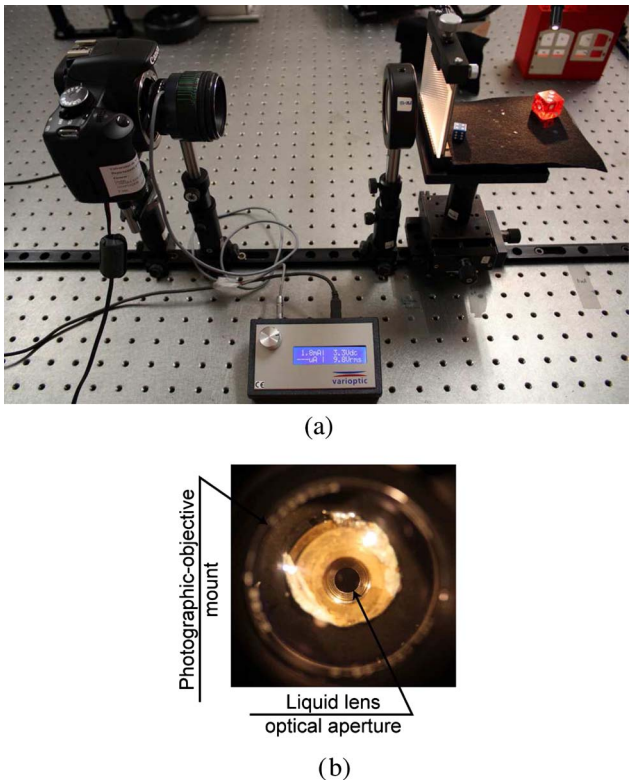

Fig. 3. (Color online) (a) Experimental setup used for the multiple-imaging experiment. The liquid lens was inserted into the aperture-stop plane of the camera lens. The distance from the field lens to the camera lens was adjusted so that the system is telecentric. By placing the microlens array in front of the field lens, a collection of elemental images of the 3D scenes was obtained. (b) Image of the variable-focal-length lens mount, obtained by means of an auxiliary digital camera.

APPENDIX A

The same result as in Section 3 could be achieved by projecting the optical power of the liquid lens onto the front focal plane of any microlens. To do that, we have to take into account that the amplitude transmittance of a spherical lens can be expressed as [26]

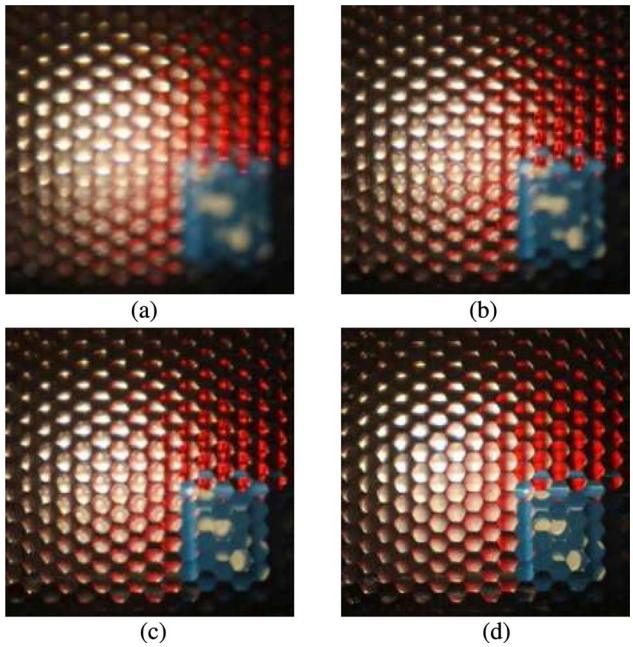

Fig. 4. (Color online) Four frames of a movie (Media 1) obtained after continuously modifying the optical power of the variable-focal-length lens. (a) The parallel-imaging system focuses farther than the red die. (b) The focus is on the red die. (c) Intermediate focusing. (d) The focus is on the blue die.

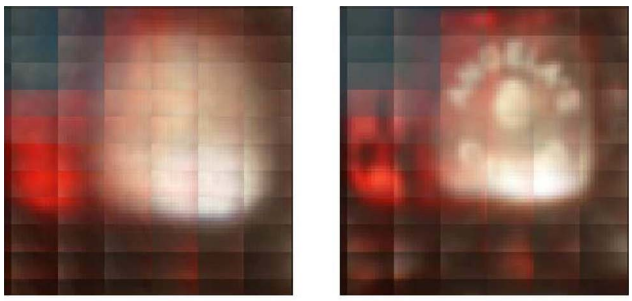

(a) (b)

Fig. 5. (Color online) Reconstructed field calculated by projecting the integral images of Figs. 4(a) and 4(b) through the corresponding pinhole array. Optical barriers were also simulated to avoid overlapping.

$$t_{\mathrm{L}}(x,y) = \exp\left\{-i\frac{\pi\varphi_{\mathrm{L}}}{\lambda}(x^2+y^2)\right\}. \tag{A1}$$

This transmittance is backprojected, virtually, into the front focal plane of any microlens with scaling factor

$$M_{\mathrm{p}} = -f_{\mathrm{m}}/f_{\mathrm{F}}, \tag{A2}$$

so that the projected transmittance, t_{PL}, is

$$t_{\mathrm{PL}}(x,y) = t_L\left(\frac{x}{M_{\mathrm{p}}},\frac{y}{M_{\mathrm{p}}}\right) = \exp\left\{-i\frac{\pi\varphi_{\mathrm{L}}}{\lambda M_{\mathrm{p}}^2}(x^2+y^2)\right\}. \tag{A3}$$

Thus, the projected optical power, φ_{PL}, is

$$\varphi_{\mathrm{PL}} = \frac{f_{\mathrm{F}}^2}{f_{\mathrm{m}}^2}\varphi_{\mathrm{L}}. \tag{A4}$$

The coupling between any microlens and the back-projected power is equivalent to a new microlens whose focal length, f_{mN}, is just equal to the microlens focal length f_{m}. As shown in Fig. 6, the front focus of the coupling, F_{mN}, is still at the same position, whereas F'_{mN} is now at a distance $f_{\mathrm{m}}-f_{\mathrm{m}}^2\varphi_{\mathrm{PL}}=f_{\mathrm{m}}-f_{\mathrm{F}}^2\varphi_L$ from the microlens. Considering again, as in Section 3, that the distance between the camera lens and the sensor remains fixed, we can write

$$z'_{\mathrm{N}} = z' + f_{\mathrm{F}}^2\varphi_{\mathrm{L}} \tag{A5}$$

and straightforwardly obtain Eqs. (7) and (8) of Section 3.

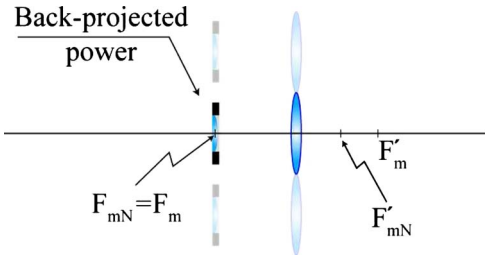

Fig. 6. (Color online) Scheme of the coupling between any microlens and the projected power. Whereas the total power and the position of the front focal planes do not change, the back focal plane is shifted toward the microlens.

ACKNOWLEDGMENTS

This work has been funded in part by the Plan Nacional I+D+I, Ministerio de Ciencia e Innovación (Spain) through grant FIS2009-9135 and by the Generalitat Valenciana (Spain) through grants GVPRE/2008/295 and PROMETEO2009-077. A. Tolosa gratefully acknowledges financial support from IMPIVA (grant IMDITS/2009/4), Generalitat Valenciana, Spain.

REFERENCES

1. M. G. Lippmann, "Epreuves reversibles donnant la sensation du relief," J. Phys. (France) **7**, 821–825 (1908).
2. C. B. Burckhardt, "Optimum parameters and resolution limitation of Integral Photography," J. Opt. Soc. Am. **58**, 71–76 (1968).
3. T. Okoshi, "Three-dimensional displays," Proc. IEEE **68**, 548–564 (1980).
4. J. Arai, F. Okano, H. Hoshino, and I. Yuyama, "Gradient-index lens-array method based on real-time integral photography for three-dimensional images," Appl. Opt. **37**, 2034–2045 (1998).
5. H. Arimoto and B. Javidi, "Integral 3D imaging with digital reconstruction," Opt. Lett. **26**, 157–159 (2001).
6. R. Martínez-Cuenca, G. Saavedra, M. Martínez-Corral, and B. Javidi, "Enhanced depth of field integral imaging with sensor resolution constraints," Opt. Express **12**, 5237–5242 (2004).
7. R. Martínez-Cuenca, G. Saavedra, M. Martínez-Corral, and B. Javidi, "Extended depth-of-field 3-D display and visualization by combination of amplitude-modulated microlenses and deconvolution tools," J. Disp. Technol. **1**, 321–327 (2005).
8. J.-S. Jang and B. Javidi, "Three-dimensional synthetic aperture integral imaging," Opt. Lett. **27**, 1144–1146 (2002).
9. J.-S. Jang and B. Javidi, "Large depth-of-focus time-multiplexed three-dimensional integral imaging by use of lenslets with nonuniform focal lengths and aperture sizes," Opt. Lett. **28**, 1924–1926 (2003).
10. R. Martínez-Cuenca, A. Pons, G. Saavedra, M. Martínez-Corral, and B. Javidi, "Optically-corrected elemental images for undistorted integral image display," Opt. Express **14**, 9657–9663 (2006).
11. J.-S. Jang and B. Javidi, "Improved viewing resolution of three-dimensional integral imaging by use of nonstationary micro-optics," Opt. Lett. **27**, 324–326 (2002).
12. J. Arai, M. Okui, T. Yamashita, and F. Okano, "Integral three-dimensional television using a 2000-scanning-line video system," Appl. Opt. **45**, 1704–1712 (2006).
13. S. Jung, J.-H. Park, H. Choi, and B. Lee, "Viewing-angle-enhanced integral three-dimensional imaging along all directions without mechanical movement," Opt. Express **12**, 1346–1356 (2003).
14. R. Martínez-Cuenca, H. Navarro, G. Saavedra, B. Javidi, and M. Martínez-Corral, "Enhanced viewing-angle integral imaging by multiple-axis telecentric relay system," Opt. Express **15**, 16255–16260 (2007).
15. J.-H. Park, H.-R. Kim, Y. Kim, J. Kim, J. Hong, S.-D. Lee, and B. Lee, "Depth-enhanced three-dimensional two-dimensional convertible display based on modified integral imaging," Opt. Lett. **29**, 2734–2736 (2004).
16. S.-H. Hong, J.-S. Jang, and B. Javidi, "Three-dimensional volumetric object reconstruction using computational integral imaging," Opt. Express **12**, 483–491 (2004).
17. C. Wu, A. Aggoun, M. McCormick, and S. Y. Kung, "Depth measurement from integral images through viewpoint image extraction and a modified multibaseline disparity analysis algorithm," J. Electron. Imaging **14**, 023018 (2005).
18. A. Stern and B. Javidi, "3D image sensing, visualization, and processing using integral Imaging," Proc. IEEE **94**, 591–608 (2006).

19. R. Martinez-Cuenca, G. Saavedra, M. Martinez-Corral, and B. Javidi "Progress in 3-D multiperspective display by integral imaging," Proc. IEEE **97**, 1067–1077 (2009).
20. B. Javidi, F. Okano, and J. Y. Son, *Three-Dimensional Imaging, Visualization, and Display* (Springer, 2009).
21. L. Miccio, A. Finizio, S. Grilli, V. Vespini, M. Paturzo, S. De Nicola, and P. Ferraro, "Tunable liquid microlens arrays in electrode-less configuration and their accurate characterization by interference microscopy," Opt. Express **17**, 2487–2499 (2009).
22. R. S. Longhurst, *Geometrical and Physical Optics* (Longman, 1973), Chap. 2.
23. C. Quillet and B. Berge, "Electrowetting: a recent outbreak," Curr. Opin. Colloid Interface Sci. **6**, 34–39 (2001).
24. B. Berge and J. Peseux, "Variable focal lens controlled by an external voltage: an application of electrowetting," Eur. Phys. J. E **3**, 59–163 (2000).
25. C. Gabay, B. Berge, G. Dovillaire, and S. Bucourt, "Dynamic study of a Varioptic variable focal lens," Proc. SPIE **4767**, 159–165 (2002).
26. J. W. Goodman, *Introduction to Fourier Optics* (McGraw-Hill, 1996).